

A tuning algorithm for a sliding mode controller of buildings with ATMD

Antonio Concha^a, Suresh Thenozhi^b, Ramón Octavio Jiménez Betancourt^c, S. K. Gadi^{d,*}

^aFacultad de Ingeniería Mecánica y Eléctrica, Universidad de Colima, Coquimatlán, Colima 28400, México

^bFacultad de Ingeniería, Universidad Autónoma de Querétaro, Santiago de Querétaro, Querétaro 76010, México

^cFacultad de Ingeniería Electromecánica, Universidad de Colima, Manzanillo, Colima 28860, México

^dFacultad de Ingeniería Mecánica y Eléctrica, Universidad Autónoma de Coahuila, Torreón, Coahuila 27276, México

Abstract

This paper proposes an automatic tuning algorithm for a sliding mode controller (SMC) based on the Ackermann's formula, that attenuates the structural vibrations of a seismically excited building equipped with an Active Tuned Mass Damper (ATMD) mounted on its top floor. The switching gain and sliding surface of the SMC are designed through the proposed tuning algorithm to suppress the structural vibrations by minimizing either the top floor displacement or the control force applied to the ATMD. Moreover, the tuning algorithm selects the SMC parameters to guarantee the following closed-loop characteristics: 1) the transient responses of the structure and the ATMD are sufficiently fast and damped; and 2) the control force, as well as the displacements and velocities of the building and ATMD are within acceptable limits under the frequency band of the earthquake excitation. The proposed SMC shows robustness against the unmodeled dynamics such as the friction of the damper. Experimental results on a reduced scale structure permits demonstrating the efficiency of the tuning algorithm for the SMC, which is compared with the traditional Linear Quadratic Regulator (LQR).

1. Introduction

Buildings can be subject to external forces such as earthquakes or winds, which can damage them. To protect the buildings against these natural events, they can be coupled to Mass Dampers (MD) to obtain a desired vibration attenuation. The passive version of the MD, known as Tuned Mass Dampers (TMD), are composed of a moving mass attached to a spring and a viscous damper. If the damper also has Coulomb-type dissipation force, then it can be denoted as FTMD [1]. The active version, termed as Active Mass Damper (AMD), are constructed by coupling an actuator to the moving mass. By adding an actuator to the TMD results in a hybrid device, denoted as ATMD [2].

Active vibration control techniques using AMD or ATMD have been of great interest in recent years, due to their ability to provide higher vibration attenuation than the TMD. Linear controllers are by far the most widely applied techniques for active vibration control. They include the classical proportional-derivative (PD) or the proportional-integral-derivative (PID) controllers [3, 4]; acceleration feedback regulators [5, 6]; state-feedback with variable gain [7]; full state feedback control using displacement, velocity, and acceleration of the structure [8–11]; LQR using the knowledge of the seismic excitation [12, 13] or without it [14]; Linear Quadratic Gaussian (LQG) [15]; feedforward and feedback optimal tracking controller (FFOTC) [16]; and robust controllers like H_2 , H_∞ [17, 18] or H_2/H_∞ [19]. On the other hand, intelligent techniques have also been applied for active control of structures. Yang et al. [20] designed a neural-network for system identification and vibration control of a structure with AMD. Thenozhi and Yu [21] designed Fuzzy

*Corresponding author

Email addresses: aconcha@ucol.mx (Antonio Concha), suresh@uaq.mx (Suresh Thenozhi), rjimenez@ucol.mx (Ramón Octavio Jiménez Betancourt), Research@SKGadi.com (S. K. Gadi)

PD/PID controllers for structures with friction uncertainty. Genetic algorithms were applied in [22, 23] for optimization of structural active control laws.

An alternative to the aforementioned linear and intelligent control techniques is the SMC, that is widely accepted for structural control due to its robustness against disturbances and unmodeled dynamics. Yang et al. [24] presented a continuous SMC based on a saturation function for seismically excited structures, where the authors showed with numerical simulations that this controller avoids the undesirable chattering effect. Adhikari et. al [25] designed a SMC based on the theory of compensators to prevent a large response in the building due to its interaction with the ATMD. On the other hand, Wang et al. [26] developed a fuzzy SMC that uses a Mamdani inference method to determine the behavior of the closed-loop system in the sliding mode. Moreover, Li et. al [27] proposed a model reference SMC for a building with an ATMD at its top floor, where the reference model is the structure coupled to the TMD. Soleymani et al. [28] designed a SMC for a building modeled through a second-order reduced model, and they consider time delays in the control force applied to an AMD coupled to the structure. In addition, Mamat et al. [29] presented an adaptive nonsingular terminal SMC employed in a three-story building equipped with an ATMD, that was simulated in Matlab/Simulink.

This article proposes an algorithm to automatically tune the sliding variable and switching gain of a SMC based on the Ackermann's formula, that is used for vibration control of a building containing an ATMD on its top floor. Considering that the first mode of the building response is dominant during the earthquake, the structure equipped with the ATMD is modeled as a fourth-order system. It is shown that the closed-loop system in the sliding mode is reduced to a third-order system, whose displacement of the dominant mode of the structure and that of the ATMD damper, as well as its control force behaves as the outputs of a dominant second-order filters, whose input is the seismic excitation. These filters have the advantage that are easier to design than the four-order filters presented in [5]. The aim of the proposed tuning algorithm is to design these dominant second-order filters to:

- minimize the displacement of the top floor of the structure as much as possible, or to minimize the control force applied to the ATMD while offering a great attenuation of this displacement.
- produce sufficiently fast and damped transient responses of the ATMD and building.
- guarantee that the Root Mean Square (RMS) values of the ATMD control force, displacements and velocities of the building and damper are within acceptable limits in the frequency band of the earthquake excitation.

Unlike the SMC techniques presented in [24–29], this article proves that the seismic excitation signal is not a coupled disturbance, whose effect on the controller and on the movements of the ATMD and building is analyzed. Moreover, in contrast to [25], that uses a compensator to filter out undesirable ATMD responses, the present work uses the dominant second-order filters to remove these undesirable responses, which are automatically designed using the proposed tuning algorithm. Thus, large responses in the building due to the movements of the ATMD are avoided.

The remaining of this paper is organized as follows. Section 2 introduces the mathematical model of a building equipped with an ATMD. The SMC designed with the Ackermann's formula is presented in Section 3. The desired transient and frequency responses of the closed-loop structure are described in Section 4. The proposed algorithm for tuning the sliding variable and switching gain of the SMC is explained in Section 5. Section 6 demonstrates the effectiveness of the proposed tuning algorithm in both simulations and experiments. Finally, Section 7 gives the conclusions of this article.

2. Mathematical model of a building with an ATMD

Consider a N -story building that has an ATMD installed at its top floor, as shown in Figure 1. The behavior of this system is described by means of the following differential equations [30, 31]:

$$\mathbf{M}(\ddot{\mathbf{x}}(t) + \mathbf{l}\ddot{x}_g(t)) + \mathbf{C}\dot{\mathbf{x}}(t) + \mathbf{K}\mathbf{x}(t) = -\mathbf{\Gamma}F(t) \quad (1)$$

$$m_d(\ddot{x}_n(t) + \ddot{x}_g(t) + \ddot{x}_d(t)) = F(t) \quad (2)$$

$$F(t) = u(t) - k_d x_d(t) - c_d \dot{x}_d(t) - f(\dot{x}_d(t)) \quad (3)$$

where $\mathbf{M}, \mathbf{C}, \mathbf{K} \in \mathbb{R}^{N \times N}$ are the mass, stiffness, and damping matrices, respectively. Term \mathbf{M} is a diagonal matrix composed by the floor masses m_i , $i = 1, 2, \dots, N$. Moreover, \mathbf{C} and \mathbf{K} are tridiagonal matrices that contain the damping c_i and stiffness k_i coefficients between the i th and the $(i - 1)$ th floors, as depicted in Figure 1. Furthermore, the term \ddot{x}_g is the earthquake acceleration, vector \mathbf{x} is given by $\mathbf{x} = [x_1, x_2, \dots, x_N]^T$, where x_i represents the displacement of the i th floor relative to the ground. Variable x_d is the relative displacement of the ATMD with respect to the top story, and the terms m_d , k_d , c_d , and $f(\dot{x}_d(t))$ are the mass, stiffness, damping, and non-linear friction of the ATMD, respectively. Variable F is the net force acting upon the ATMD. In addition, signal $u(t)$ is the control force applied to the damper, term $\mathbf{l} \in \mathbb{R}^{N \times 1}$ is an unity vector, and $\mathbf{\Gamma} \in \mathbb{R}^{N \times 1}$ defines the localization of the ATMD and is represented as:

$$\mathbf{\Gamma} = [0, 0, \dots, 0, 1]^T \quad (4)$$

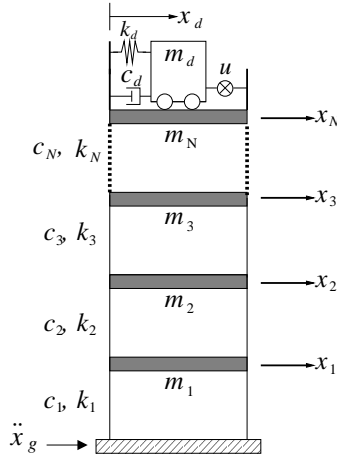


Figure 1: Building structure equipped with an ATMD mounted on its top floor.

Since the first mode of vibration is dominant during an earthquake, the building model (1) can be approximated as [8]:

$$\begin{aligned} m_0 \ddot{x}_0(t) + c_0 \dot{x}_0(t) + k_0 x_0(t) &= -\beta_0 m_0 \ddot{x}_g(t) - F(t) \\ m_d (\ddot{x}_0(t) + \ddot{x}_g(t) + \ddot{x}_d(t)) &= F(t) \end{aligned} \quad (5)$$

Signal x_0 represents the displacement of the dominant mode, which is given by

$$x_0(t) = \frac{\phi_0^T \mathbf{M} \mathbf{x}(t)}{\phi_0^T \mathbf{M} \phi_0} \quad (6)$$

where $\phi_0 \in \mathbb{R}^{N \times 1}$ is the first mode, that is scaled to satisfy

$$\phi_0^T \mathbf{\Gamma} = 1 \quad (7)$$

This equality, in turn, produces the approximation [32]

$$x_N(t) \approx x_0(t) \quad (8)$$

Parameters m_0 , c_0 , k_0 , and β_0 are the mass, damping, stiffness, and participation factor of the dominant mode, respectively. They are defined as [30]:

$$m_0 = \phi_0^T \mathbf{M} \phi_0, \quad c_0 = \phi_0^T \mathbf{C} \phi_0, \quad k_0 = \phi_0^T \mathbf{K} \phi_0, \quad \beta_0 = \frac{\phi_0^T \mathbf{M} \mathbf{l}}{\phi_0^T \mathbf{M} \phi_0} \quad (9)$$

Moreover, the natural frequency of the first mode is given by

$$\omega_0 = \sqrt{\frac{k_0}{m_0}} \quad (10)$$

Using the approximation (8) and substituting $F(t)$ of (3) into (5) yields:

$$\begin{aligned} \ddot{x}_N &= -\frac{c_0}{m_0} \dot{x}_N - \frac{k_0}{m_0} x_N - \beta_0 \ddot{x}_g + \frac{c_d}{m_0} \dot{x}_d + \frac{f(\dot{x}_d)}{m_0} + \frac{k_d}{m_0} x_d - \frac{1}{m_0} u \\ \ddot{x}_d &= \left(\frac{m_0 + m_d}{m_0 m_d} \right) (u - c_d \dot{x}_d - f(\dot{x}_d) - k_d x_d) + \frac{k_0}{m_0} x_N + \frac{c_0}{m_0} \dot{x}_N + \ddot{x}_g (\beta_0 - 1) \end{aligned} \quad (11)$$

where argument t has been omitted in the time dependent signals.

Defining the following state variables

$$z_1 = x_d, \quad z_2 = x_N, \quad z_3 = \dot{x}_d, \quad z_4 = \dot{x}_N \quad (12)$$

allows rewriting system (11) in the following state-space representation:

$$\begin{aligned} \underbrace{\begin{bmatrix} \dot{z}_1 \\ \dot{z}_2 \\ \dot{z}_3 \\ \dot{z}_4 \end{bmatrix}}_{\dot{\mathbf{z}}} &= \underbrace{\begin{bmatrix} 0 & 0 & 1 & 0 \\ 0 & 0 & 0 & 1 \\ -\frac{k_d(m_0 + m_d)}{m_0 m_d} & \frac{k_0}{m_0} & -\frac{c_d(m_0 + m_d)}{m_0 m_d} & \frac{c_0}{m_0} \\ \frac{k_d}{m_0} & -\frac{k_0}{m_0} & \frac{c_d}{m_0} & -\frac{c_0}{m_0} \end{bmatrix}}_{\mathbf{A}} \underbrace{\begin{bmatrix} z_1 \\ z_2 \\ z_3 \\ z_4 \end{bmatrix}}_{\mathbf{z}} \\ &+ \underbrace{\begin{bmatrix} 0 \\ 0 \\ \frac{(m_0 + m_d)}{m_0 m_d} \\ -\frac{1}{m_0} \end{bmatrix}}_{\mathbf{B}} (u - f(z_3)) + \underbrace{\begin{bmatrix} 0 \\ 0 \\ \beta_0 - 1 \\ -\beta_0 \end{bmatrix}}_{\mathbf{D}} \ddot{x}_g \end{aligned} \quad (13)$$

3. Sliding mode control of the structure

This section presents a SMC design based on the Ackermann's formula for vibration attenuation of seismically excited buildings. For this purpose, let us first define a full-state feedback controller u_a for system (13), such that the closed-loop eigenvalues λ_1 , λ_2 , λ_3 , and λ_4 are placed in a desired location in the s -plane. The control law u_a is given by

$$u_a = -\mathbf{k}^T \mathbf{z} \quad (14)$$

According to the Ackermann's formula [33], the feedback gain vector $\mathbf{k}^T \in \mathbb{R}^{1 \times 4}$ can be computed as

$$\mathbf{k}^T = \mathbf{e}^T P(\mathbf{A}) \quad (15)$$

with

$$\mathbf{e}^T = [0, 0, 0, 1][\mathbf{B}, \mathbf{A}\mathbf{B}, \mathbf{A}^2\mathbf{B}, \mathbf{A}^3\mathbf{B}]^{-1} \in \mathbb{R}^{1 \times 4} \quad (16)$$

$$P(\lambda) = (\lambda - \lambda_1)(\lambda - \lambda_2)(\lambda - \lambda_3)(\lambda - \lambda_4) \quad (17)$$

In order to design the SMC for the system (13), let us consider the following assumptions:

Assumption 1. *The eigenvalue λ_4 in (17) is real and negative.*

Assumption 2. *Bounds δ and ϖ , corresponding to the earthquake acceleration \ddot{x}_g and the non-linear friction $f(z_3)$, respectively, are known and satisfy*

$$|\ddot{x}_g| \leq \delta \quad (18)$$

$$|f(z_3)| \leq \varpi \quad (19)$$

where the bound δ can be determined from the historical records of the ground acceleration in the region where the building is located, and the bound ϖ can be determined using friction estimation techniques.

Next theorem presents the SMC based on the Ackermann's formula (15) and analyses the behavior of the resulting closed-loop system in the sliding mode at the plane $\sigma = \boldsymbol{\eta}^T \mathbf{z} = 0$, where $\boldsymbol{\eta}^T \in \mathbb{R}^{1 \times 4}$ is a constant vector that will be automatically calculated through the proposed methodology outlined in Section 5.

Theorem 3.1. *Let us consider the building structure in (13), that is equipped with an ATMD, whose control force u is provided by the following SMC*

$$u = -M_0 \text{sign}(\sigma) \quad (20)$$

where $\sigma = \boldsymbol{\eta}^T \mathbf{z}$ and $M_0 > 0$ are called sliding variable and switching gain, respectively. The vector $\boldsymbol{\eta}^T$ is given by

$$\boldsymbol{\eta}^T = [\eta_1, \eta_2, \eta_3, \eta_4] = \mathbf{e}^T P_1(\mathbf{A}), \quad P_1(\lambda) = (\lambda - \lambda_1)(\lambda - \lambda_2)(\lambda - \lambda_3) \quad (21)$$

where λ_1, λ_2 , and λ_3 are the desired closed-loop eigenvalues; moreover, parameter M_0 satisfies

$$M_0 > \varpi + h_0 \quad (22)$$

where h_0 is a constant such that

$$|u_a + \alpha_1 \ddot{x}_g| \leq h_0 \quad (23)$$

with u_a given in (14) and α_1 defined as

$$\alpha_1 = \beta_0(\eta_4 - \eta_3) + \eta_3 \quad (24)$$

Then, the trajectories of closed-loop system reach the plane $\sigma = \boldsymbol{\eta}^T \mathbf{z} = 0$ in a finite time t_σ , and they are confined in this plane for $t \geq t_\sigma$, where $t_\sigma \leq \sigma(0)/(M_0 - [\varpi + h_0])$. Furthermore, when this plane is reached, the fourth-order dynamic system (13) is reduced to the following third-order system

$$\dot{\mathbf{z}}^* = \mathbf{A}_1 \mathbf{z}^* + \mathbf{B}_1 \ddot{x}_g \quad (25)$$

where $\mathbf{A}_1 \in \mathbb{R}^{3 \times 3}$ is a matrix containing the eigenvalues λ_1, λ_2 , and λ_3 ; vector $\mathbf{z}^* \in \mathbb{R}^{3 \times 1}$ is given by

$$\mathbf{z}^* = [z_1, z_2, z_3]^T \quad (26)$$

and

$$\mathbf{B}_1 = \begin{pmatrix} 0 \\ 0 \\ \alpha_2 \end{pmatrix} \quad \text{with} \quad \alpha_2 = (\beta_0 - 1) + \frac{\alpha_1(m_0 + m_d)}{m_0 m_d} \quad (27)$$

Proof. First, note that vector $\boldsymbol{\eta}^T$ in (21) satisfies the following equalities [34]:

$$\boldsymbol{\eta}^T \mathbf{B} = 1, \quad \boldsymbol{\eta}^T \mathbf{A}^* = \lambda_4 \boldsymbol{\eta}^T \quad (28)$$

where $\mathbf{A}^* = \mathbf{A} - \mathbf{B}\mathbf{k}^T$.

Adding and subtracting the term $\mathbf{B}u_a$ to (13) yields

$$\dot{\mathbf{z}} = (\mathbf{A} - \mathbf{B}\mathbf{k}^T)\mathbf{z} + \mathbf{B}[u - u_a - f(z_3)] + \mathbf{D}\ddot{x}_g \quad (29)$$

The system (29) is transformed into a new set of equations using the following state transformation

$$\mathbf{w} = \begin{bmatrix} \mathbf{z}^* \\ \sigma \end{bmatrix} = \overbrace{\begin{bmatrix} \mathbf{I}_{3 \times 3} & \mathbf{0}_{3 \times 1} \\ \boldsymbol{\eta}^T & \end{bmatrix}}^{\mathbf{T}} \mathbf{z} = \mathbf{T}\mathbf{z} \quad (30)$$

where \mathbf{T} is an invertible matrix. The dynamics of the transformed system $\dot{\mathbf{w}} = \mathbf{T}\dot{\mathbf{z}}$ is given by

$$\begin{aligned} \dot{\mathbf{w}} &= \mathbf{T}((\mathbf{A} - \mathbf{B}\mathbf{k}^T)\mathbf{z} + \mathbf{B}[u - u_a - f(z_3)] + \mathbf{D}\ddot{x}_g) \\ &= \mathbf{T}(\mathbf{A} - \mathbf{B}\mathbf{k}^T)\mathbf{T}^{-1}\mathbf{w} + \mathbf{TB}[u - u_a - f(z_3)] + \mathbf{TD}\ddot{x}_g \end{aligned} \quad (31)$$

Using the equalities in (28) allows deducing the following structure of matrices $\mathbf{T}(\mathbf{A} - \mathbf{B}\mathbf{k}^T)\mathbf{T}^{-1}$ and \mathbf{TB} in (31)

$$\mathbf{T}(\mathbf{A} - \mathbf{B}\mathbf{k}^T)\mathbf{T}^{-1} = \begin{bmatrix} \mathbf{A}_1 & \mathbf{a}^* \\ \mathbf{0}_{1 \times 3} & \lambda_4 \end{bmatrix}, \quad \mathbf{TB} = \begin{bmatrix} \mathbf{b}^* \\ 1 \end{bmatrix} \quad \text{with} \quad \mathbf{b}^* = \begin{pmatrix} 0 \\ 0 \\ \frac{(m_0 + m_d)}{m_0 m_d} \end{pmatrix} \quad (32)$$

where $\mathbf{a}^* \in \mathbb{R}^{3 \times 1}$, and \mathbf{A}_1 is a matrix whose eigenvalues are equal to the closed-loop eigenvalues λ_1, λ_2 and λ_3 . Finally, vector \mathbf{TD} in (31) is given by

$$\mathbf{TD} = \begin{bmatrix} \mathbf{d}_1 \\ -\alpha_1 \end{bmatrix} \quad \text{with} \quad \mathbf{d}_1 = \begin{pmatrix} 0 \\ 0 \\ \beta_0 - 1 \end{pmatrix} \quad (33)$$

Substituting equations (32) and (33) into (31) produces

$$\dot{\mathbf{z}}^* = \mathbf{A}_1 \mathbf{z}^* + \mathbf{a}^* \sigma + \mathbf{b}^* [u - u_a - f(z_3)] + \mathbf{d}_1 \ddot{x}_g \quad (34)$$

$$\dot{\sigma} = \lambda_4 \sigma + u - u_a - f(z_3) - \alpha_1 \ddot{x}_g \quad (35)$$

The control law u is designed so that the trajectories of the structural system (13) converge to the plane $\sigma = 0$ in finite time, which is ensured when $\frac{1}{2} \frac{d}{dt} \sigma^2 = \sigma \dot{\sigma} < 0$. The product $\sigma \dot{\sigma}$ is given by

$$\sigma \dot{\sigma} = \sigma [\lambda_4 \sigma + u - u_a - f(z_3) - \alpha_1 \ddot{x}_g] = \lambda_4 \sigma^2 + \sigma [u - u_a - f(z_3) - \alpha_1 \ddot{x}_g] \quad (36)$$

Since $\lambda_4 < 0$, the last expression satisfies

$$\sigma \dot{\sigma} \leq \sigma [u - u_a - f(z_3) - \alpha_1 \ddot{x}_g] \quad (37)$$

Substituting the control law $u = -M_0 \text{sign}(\sigma)$ into (37), and using the inequalities (19), (22) and (23) yields

$$\sigma \dot{\sigma} \leq \sigma [-M_0 \text{sign}(\sigma) - u_a - f(z_3) - \alpha_1 \ddot{x}_g] \leq |\sigma| [-M_0 + \varpi + h_0] \leq -|\sigma| [M_0 - (\varpi + h_0)] < 0 \quad (38)$$

Therefore, the trajectories of system (13) reach the surface $\sigma = \boldsymbol{\eta}^T \mathbf{z} = 0$ in a finite time t_σ , and remain there for $t \geq t_\sigma$, where t_σ is computed by integrating (38) and its value is given by

$$t_\sigma \leq \frac{\sigma(0)}{M_0 - (\varpi + h_0)} \quad (39)$$

Finally, in order to determine the behavior of the closed-loop system in the surface $\sigma = 0$, the next solution of $\dot{\sigma} = 0$ with respect to u

$$u = u_a + f(z_3) + \alpha_1 \ddot{x}_g \quad (40)$$

is substituted into (34) to produce the sliding motion equation (25). \square

Remark Since the SMC (20) and the dynamics of the closed-loop system (25) in the sliding mode do not depend of λ_4 , this parameter can take any negative value, and it is used only for the stability analysis of the SMC.

Remark Note that the building and the ATMD are at rest before an earthquake, therefore, the initial condition $z_i(0)$ of variables z_i , $i = 1, 2, 3, 4$ is zero, i.e., $\mathbf{z}(0) = \mathbf{0}$, which implies that $\sigma(0) = \boldsymbol{\eta}^T \mathbf{z}(0) = 0$, and as an consequence $t_\sigma = 0$.

Remark Parameter h_0 in (23) is required to design the SMC. In section 5.2, a methodology is proposed to compute this parameter using the frequency response of the closed-loop system in the sliding mode, and the knowledge of the bound δ in (18) of the earthquake acceleration \ddot{x}_g .

4. Analysis of the closed-loop system at the sliding mode

The closed-loop system dynamics in the sliding mode is described in the Laplace domain as

$$(s\mathbf{I}_{3 \times 3} - \mathbf{A}_1)\mathbf{Z}^*(s) = \mathbf{B}_1 \mathcal{L}[\ddot{x}_g(t)] \quad (41)$$

where \mathcal{L} is the Laplace transform operator and $\mathbf{Z}^*(s) = [Z_1(s), Z_2(s), Z_3(s)]^T$.

Using (41), the transfer function $\mathbf{Z}^*(s)/\mathcal{L}[\ddot{x}_g(t)]$ can be expressed as

$$\frac{\mathbf{Z}^*(s)}{\mathcal{L}[\ddot{x}_g(t)]} = (s\mathbf{I}_{3 \times 3} - \mathbf{A}_1)^{-1} \mathbf{B}_1 \quad (42)$$

The characteristic polynomial $P_1(s)$ in (21) corresponding to (42) can be rewritten as

$$P_1(s) = (s - \lambda_1)(s - \lambda_2)(s - \lambda_3) = (s^2 + 2\zeta\omega_n s + \omega_n^2)(s - \lambda_3) \quad (43)$$

where ζ and ω_n are positive constants, which are called damping ratio and undamped natural frequency, respectively.

Substituting $P_1(s)$ into (42) leads to the following transfer functions $Z_1(s)/\mathcal{L}[\ddot{x}_g(t)]$, $Z_2(s)/\mathcal{L}[\ddot{x}_g(t)]$ and $Z_3(s)/\mathcal{L}[\ddot{x}_g(t)]$:

$$G_1(s) = \frac{Z_1(s)}{\mathcal{L}[\ddot{x}_g(t)]} = \mathbf{C}_{z_1}(s\mathbf{I}_{3 \times 3} - \mathbf{A}_1)^{-1} \mathbf{B}_1 = \frac{\alpha_2(s - \psi_1)}{(s - \lambda_3)(s^2 + 2\zeta\omega_n s + \omega_n^2)} \quad (44)$$

$$G_2(s) = \frac{Z_2(s)}{\mathcal{L}[\ddot{x}_g(t)]} = \mathbf{C}_{z_2}(s\mathbf{I}_{3 \times 3} - \mathbf{A}_1)^{-1} \mathbf{B}_1 = \frac{-\alpha_2\eta_3(s - \psi_2)}{\eta_4(s - \lambda_3)(s^2 + 2\zeta\omega_n s + \omega_n^2)} \quad (45)$$

$$G_3(s) = \frac{Z_3(s)}{\mathcal{L}[\ddot{x}_g(t)]} = \mathbf{C}_{z_3}(s\mathbf{I}_{3 \times 3} - \mathbf{A}_1)^{-1} \mathbf{B}_1 = \frac{\alpha_2 s(s - \psi_1)}{(s - \lambda_3)(s^2 + 2\zeta\omega_n s + \omega_n^2)} \quad (46)$$

where

$$\psi_1 = -\frac{\eta_2}{\eta_4}, \quad \psi_2 = -\frac{\eta_1}{\eta_3}, \quad (47)$$

$$\mathbf{C}_{z_1} = [1, 0, 0], \quad \mathbf{C}_{z_2} = [0, 1, 0], \quad \mathbf{C}_{z_3} = [0, 0, 1] \quad (48)$$

In order to determine the transfer function $U(s)/\mathcal{L}[\ddot{x}_g(t)]$, consider that non-linear function $f(z_3)$ in (40) is zero. Then, the control signal u in the sliding mode is given by:

$$\begin{aligned} u &= u_a + \alpha_1 \ddot{x}_g = -\mathbf{k}^T \mathbf{z} + \alpha_1 \ddot{x}_g = -\mathbf{e}^T P(\mathbf{A}) \mathbf{z} + \alpha_1 \ddot{x}_g \\ &= -\mathbf{e}^T P_1(\mathbf{A}) [\mathbf{A} - \mathbf{I}_{4 \times 4} \lambda_4] \mathbf{z} + \alpha_1 \ddot{x}_g \\ &= -\boldsymbol{\eta}^T [\mathbf{A} - \mathbf{I}_{4 \times 4} \lambda_4] \mathbf{z} + \alpha_1 \ddot{x}_g \end{aligned} \quad (49)$$

Using the state transformation equation in (30), the vector \mathbf{z} in (49) can be written as follows

$$\mathbf{z} = \mathbf{T}^{-1} \mathbf{w} = \mathbf{T}^{-1} \begin{bmatrix} \mathbf{z}^* \\ \sigma \end{bmatrix} \quad (50)$$

Since $\sigma = 0$ in the sliding mode, the above expression becomes

$$\mathbf{z} = \mathbf{T}^{-1} \begin{bmatrix} \mathbf{z}^* \\ 0 \end{bmatrix} \quad (51)$$

Substituting (51) into (49) yields

$$u = -\boldsymbol{\eta}^T [\mathbf{A} - \mathbf{I}_{4 \times 4} \lambda_4] \mathbf{T}^{-1} \begin{bmatrix} \mathbf{z}^* \\ 0 \end{bmatrix} + \alpha_1 \ddot{x}_g \quad (52)$$

Let

$$\boldsymbol{\nu} = -\boldsymbol{\eta}^T [\mathbf{A} - \mathbf{I}_{4 \times 4} \lambda_4] \mathbf{T}^{-1} = -\boldsymbol{\eta}^T \mathbf{A} \mathbf{T}^{-1} + \lambda_4 \boldsymbol{\eta}^T \mathbf{T}^{-1} = -\boldsymbol{\eta}^T \mathbf{A} \mathbf{T}^{-1} + [0, 0, 0, \lambda_4] = [\boldsymbol{\nu}_1, \nu_2] \quad (53)$$

where $\boldsymbol{\nu} \in \mathbb{R}^{1 \times 4}$, $\boldsymbol{\nu}_1 \in \mathbb{R}^{1 \times 3}$, and $\nu_2 \in \mathbb{R}$. Using this definition allows rewriting (52) as

$$u = [\boldsymbol{\nu}_1, \nu_2] \begin{bmatrix} \mathbf{z}^* \\ 0 \end{bmatrix} + \alpha_1 \ddot{x}_g = \boldsymbol{\nu}_1 \mathbf{z}^* + \alpha_1 \ddot{x}_g \quad (54)$$

Note that $\boldsymbol{\nu}_1$ is a constant vector and does not depend on λ_4 . Applying the Laplace transform to (54) and using (42) produces:

$$U(s) = \boldsymbol{\nu}_1 (s\mathbf{I}_{3 \times 3} - \mathbf{A}_1)^{-1} \mathbf{B}_1 \mathcal{L}[\ddot{x}_g(t)] + \alpha_1 \mathcal{L}[\ddot{x}_g(t)] \quad (55)$$

which can be rewritten as the following transfer function $U(s)/\mathcal{L}[\ddot{x}_g(t)]$

$$G_u(s) = \frac{U(s)}{\mathcal{L}[\ddot{x}_g(t)]} = \boldsymbol{\nu}_1 (s\mathbf{I}_{3 \times 3} - \mathbf{A}_1)^{-1} \mathbf{B}_1 + \alpha_1 \quad (56)$$

4.1. Transient response for $z_1(t)$ and $z_2(t)$

This section analyzes the transient responses of the damper and the top floor displacements $z_1(t)$ and $z_2(t)$, respectively. This analysis will permit tuning the SMC to produce sufficiently fast and damped transient responses of $z_1(t)$ and $z_2(t)$ under sudden changes in the input excitation \ddot{x}_g . For this purpose, assume that this input is a step function, and consider the following assumption:

Assumption 3. The damping ratio ζ of the characteristic polynomial $P_1(s)$ in (43) satisfies $\zeta < 1$, which implies that $P_1(s)$ has a real pole λ_3 and two complex conjugate poles λ_1 and λ_2 , i.e.,

$$P_1(s) = (s^2 + 2\zeta\omega_n s + \omega_n^2)(s - \lambda_3) = (s + \zeta\omega_n + j\omega_d)(s + \zeta\omega_n - j\omega_d)(s - \lambda_3) \quad (57)$$

$$\lambda_1 = -\zeta\omega_n - j\omega_d, \quad \lambda_2 = -\zeta\omega_n + j\omega_d \quad (58)$$

where $\omega_d = \omega_n \sqrt{1 - \zeta^2}$ is the damped natural frequency.

Taking into account Assumption 3, the transient response of $z_i(t)$, $i = 1, 2$ can be considered as the response of a standard second-order system, that is affected by the additional pole λ_3 and zero ψ_i of the transfer function $G_i(s)$. Thus, the response of $z_i(t)$, $i = 1, 2$ can be specified by means of its rise time T_r and maximum overshoot M_p . The response $z_i(t)$ is affected by the pole λ_3 and zero ψ_i [35], as described below:

- *Effect of the additional zero:* The zero ψ_i of $G_i(s)$ can either be positive or negative, and its effect on $z_i(t)$ is the following:
 1. If the zero ψ_i is negative, then it has the effect of decreasing T_r and increasing M_p of the step response $z_i(t)$, as shown in Figure 2 (a). The increase of M_p depends on the relation $\gamma_i = |\psi_i|/(\zeta\omega_n)$. The smaller the relation γ_i , the larger the increment of M_p .
 2. If the zero ψ_i is positive, then the transfer function $G_i(s)$ is non-minimum phase. In this case, the zero ψ_i slightly increases T_r and M_p of the step response $z_i(t)$, but it produces an initial drop that appears at the beginning of the response, see Figure 2 (a). The peak of this drop depends on the relation $\gamma_i = \psi_i/(\zeta\omega_n)$. The smaller the relation γ_i , the larger this peak will be.

In conclusion, the zero ψ_i , either positive or negative, has little effect on the transient response of $z_i(t)$ for $\gamma_i \geq 3$, but as γ_i decreases below 3, it has an increasing effect, especially when $\gamma_i < 1$.

- *Effect of the additional pole:* The additional pole $\lambda_3 < 0$ of $G_i(s)$ tends to increase T_r and to decrease M_p of the step response $z_i(t)$, see Figure 2 (b). The percentage of M_p is a function of $\xi = |\lambda_3|/(\zeta\omega_n)$; the larger this relation, the smaller the percentage of M_p . The pole λ_3 has little effect for $\xi \geq 3$, otherwise has an increasing effect.

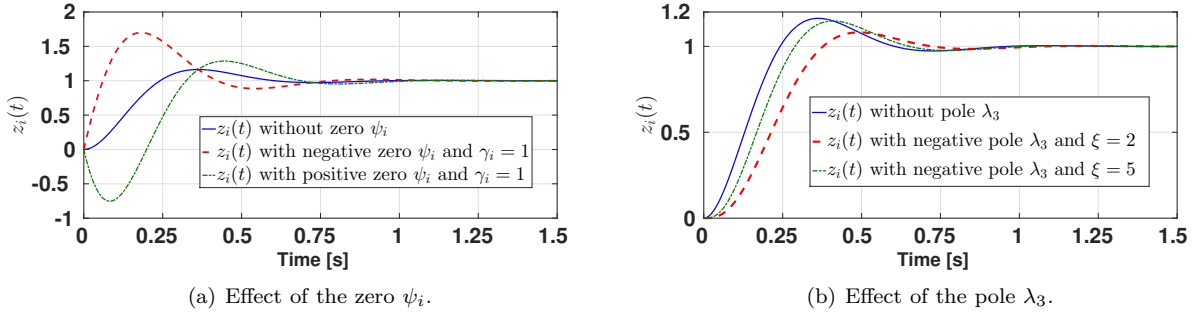


Figure 2: Effect of the additional zero and pole in the transient response of a standard second-order system with $\omega_n = 10$ rad/s and $\zeta = 0.5$.

From the above analysis, it is clear that for certain values of the additional pole and zero, they have less effect on the transient response. In that case, the parameters ζ and ω_n of the dominant underdamped second-order system are tuned such that the transient responses of $z_1(t)$ and $z_2(t)$ are sufficiently fast and damped, and they does not have excessive overshoot. To this end, the tuning of the parameters $\zeta, \omega_n, \lambda_3, \psi_1$ and ψ_2 is carried out as follows.

- The damping ratio ζ of $P_1(s)$ will be tuned between the next interval

$$\zeta_l < \zeta < \zeta_u \quad (59)$$

where the recommended values for the limits of the interval are $\zeta_l = 0.5$ and $\zeta_u = 0.9$.

- The natural frequency ω_n will be tuned based on the dominant mode frequency of the structure ω_0 . If ω_n is near to ω_0 , it could provoke abrupt movements of the ATMD that could excite the structure instead of protect it. On the other hand, if ω_n is smaller than $0.5\omega_0$ could result in a slower transient response of the ATMD movements, hence an insignificant vibration attenuation. To avoid these problems, ω_n will be tuned between the following limits

$$\omega_{nl} < \omega_n < \omega_{nu} \quad (60)$$

where $\omega_{nl} = 0.5\omega_0$ and $\omega_{nu} = 0.8\omega_0$. Moreover, the above choice help to minimize the effect of the measurement noise and unmodeled dynamics in the closed-loop system.

- To neglect the effect of the pole λ_3 on the transient responses of $z_1(t)$ and $z_2(t)$, it is fixed to:

$$\lambda_3 = -3\zeta\omega_n \quad (61)$$

- The zeros ψ_i , $i = 1, 2$ of $G_i(s)$ are selected based on the following conditions, such that they have the least possible impact on the responses z_1 and z_2 .

$$|\psi_1| \geq \gamma_1\zeta\omega_n \quad (62)$$

$$|\psi_2| \geq \gamma_2\zeta\omega_n \quad (63)$$

It is recommended to select $\gamma_1 = 5$ to guarantee that the effect of the zero ψ_1 on the ATMD displacement z_1 is insignificant. Moreover, the parameter γ_2 should be selected as large as possible, and we recommend $\gamma_2 \geq 1$.

4.2. Frequency responses of $z_1(t)$, $z_2(t)$, $z_3(t)$ and $u(t)$

The frequency responses of signals $z_1(t)$, $z_2(t)$, $z_3(t)$ and $u(t)$ will be computed to guarantee that these signals are between acceptable limits within the frequency band of $\ddot{x}_g(t)$. For that, assume that excitation signal \ddot{x}_g is a sinusoidal input, denoted as $\ddot{x}_g = \delta \sin(\omega t)$, where the amplitude δ represents the upper bound of \ddot{x}_g , as indicated in (18). Moreover, the frequency ω corresponds to the earthquake frequency with a bandwidth $\omega \in [\omega_{BWl}, \omega_{BWu}]$. Then, the steady-state of responses $z_1(t)$, $z_2(t)$, $z_3(t)$ and $u(t)$ are also sinusoids. By varying the frequency ω of \ddot{x}_g between its bandwidth permits to determine if the amplitudes of $z_1(t)$, $z_2(t)$, $z_3(t)$ and $u(t)$ are between tolerable limits within this band.

Let the transfer functions

$$H_i(s) = \delta G_i(s), \quad i = 1, 2, 3, u \quad (64)$$

where $G_1(s)$, $G_2(s)$, $G_3(s)$ and $G_u(s)$ are presented in section 4. The frequency responses of $z_1(t)$, $z_2(t)$, $z_3(t)$ and $u(t)$ are directly computed from the transfer functions $H_1(s)$, $H_2(s)$, $H_3(s)$ and $H_u(s)$ by substituting variable s by $j\omega$, where $\omega \in [\omega_{BWl}, \omega_{BWu}]$. The root mean square (RMS) value κ_i of $H_i(j\omega)$ is also calculated in the frequency band of $\ddot{x}_g(t)$. This value is defined as

$$\kappa_i = \text{RMS} \left(|H_i(j\omega)| \right)_{\omega \in [\omega_{BWl}, \omega_{BWu}]}, \quad i = 1, 2, 3, u \quad (65)$$

Since the predominant spectral content of earthquakes is between 1 to 20 Hz [36], the parameters ω_{BWl} and ω_{BWu} will be set as $\omega_{BWl} = 2\pi$ rad/s and $\omega_{BWu} = 40\pi$ rad/s.

5. Tuning algorithm for the SMC

This section presents the proposed tuning algorithm to compute: 1) the vector $\boldsymbol{\eta}$ using the transient and frequency responses of the closed-loop system; and 2) the switching gain M_0 by analyzing the frequency response $H_u(j\omega)$.

5.1. Procedure to compute vector $\boldsymbol{\eta}$

According to equation (21), vector $\boldsymbol{\eta}$ depends on the parameters ζ and ω_n of the characteristic polynomial $P_1(s)$ in (43). Let us define Υ as the possible set of vectors $\boldsymbol{\eta}$, with which the closed-loop system (25) in the sliding mode satisfies the following three conditions:

1. The limits for ζ in (59) and for ω_n in (60), the value $\lambda_3 = -3\zeta\omega_n$ for the non-dominant pole, as well as the inequalities in (62) and (63) corresponding to the zeros ψ_1 and ψ_2 , respectively.
2. The next upper limits $\bar{\kappa}_i$ for κ_i $i = 1, 2, 3$ in (65) given by

$$\kappa_i \leq \bar{\kappa}_i, \quad i = 1, 2, 3 \quad (66)$$

where $\bar{\kappa}_i$, $i = 1, 2, 3$ are positive constants, which constrain the maximum value of $|H_i(j\omega)|$ under the bandwidth $\omega \in [\omega_{BWL}, \omega_{BWu}]$, or in time-domain, the maximum permitted values of signals z_1 , z_2 and z_3 in the bandwidth of \ddot{x}_g .

3. The inequality

$$\kappa_u + \varpi \leq \bar{\kappa}_u \quad (67)$$

deduced from (40), which indicates that the sum of the RMS value κ_u of frequency response $|H_u(j\omega)|$ and the bound ϖ of the non-linear friction $f(z_3)$ should be less than or equal to the specified limit $\bar{\kappa}_u$.

Then, the vector $\boldsymbol{\eta} \in \Upsilon$ used by the SMC, denoted as $\boldsymbol{\eta}_*$, is obtained by minimizing either of the following two performance indexes (PIs)

$$J_{z_2} = \min_{\boldsymbol{\eta} \in \Upsilon} \kappa_2(\boldsymbol{\eta}) \quad (68)$$

$$J_u = \min_{\boldsymbol{\eta} \in \Upsilon} \kappa_u(\boldsymbol{\eta}) \quad (69)$$

where parameters κ_2 and κ_u show their dependency on $\boldsymbol{\eta}$. Note that J_{z_2} and J_u are related to the ability of the SMC to minimize the top floor displacement z_2 and the control force u , respectively. Hence the sliding variable $\sigma = \boldsymbol{\eta}_*^T \mathbf{z}$ guarantees a minimal of z_2 or u , while ensuring that the RMS values of the closed-loop signals are within acceptable limits and their transient responses are sufficiently fast and damped.

5.2. Procedure to compute the switching gain M_0

According to inequality (22), the value of M_0 should satisfy $M_0 > \varpi + h_0$. Among these two terms of the sum, only parameter ϖ is assumed to be known according to Assumption 2. This section presents a methodology for estimating parameter h_0 , that is subsequently employed to compute M_0 . Note that from (23), the parameter h_0 must satisfy the condition $h_0 \geq |u_a + \alpha_1 \ddot{x}_g|$, where the frequency response of the signal $u_a + \alpha_1 \ddot{x}_g$ is given by $H_u(j\omega)$. Define χ as the maximum magnitude of $|H_u(j\omega)|$ between the interval $\omega \in [\omega_{BWL}, \omega_{BWu}]$, where χ is computed using the vector $\boldsymbol{\eta}_*$ that minimizes either of the performance indexes (68) and (69), i.e.,

$$\chi = \max_{\omega \in [\omega_{BWL}, \omega_{BWu}]} (|H_u(j\omega, \boldsymbol{\eta}_*)|) \quad (70)$$

Since $\chi \geq |u_a + \alpha_1 \ddot{x}_g|$ in the spectrum of \ddot{x}_g , we will select $h_0 = \chi$. Thus, the switching gain M_0 of the SMC is computed as:

$$M_0 = \varpi + \chi + \varsigma \quad (71)$$

where ς is a small positive constant that guarantees the inequality (22), that in this work is fixed to 0.5.

Finally, Figure 3 shows the proposed tuning algorithm that computes the vector $\boldsymbol{\eta}_*$ and gain M_0 of the SMC. This algorithm implements the procedure outlined in the present section, and it is programmed in the Matlab software. The terms Δ_ζ and Δ_{ω_n} in this algorithm represent the increments for ζ and ω_n from their lower to upper limits.

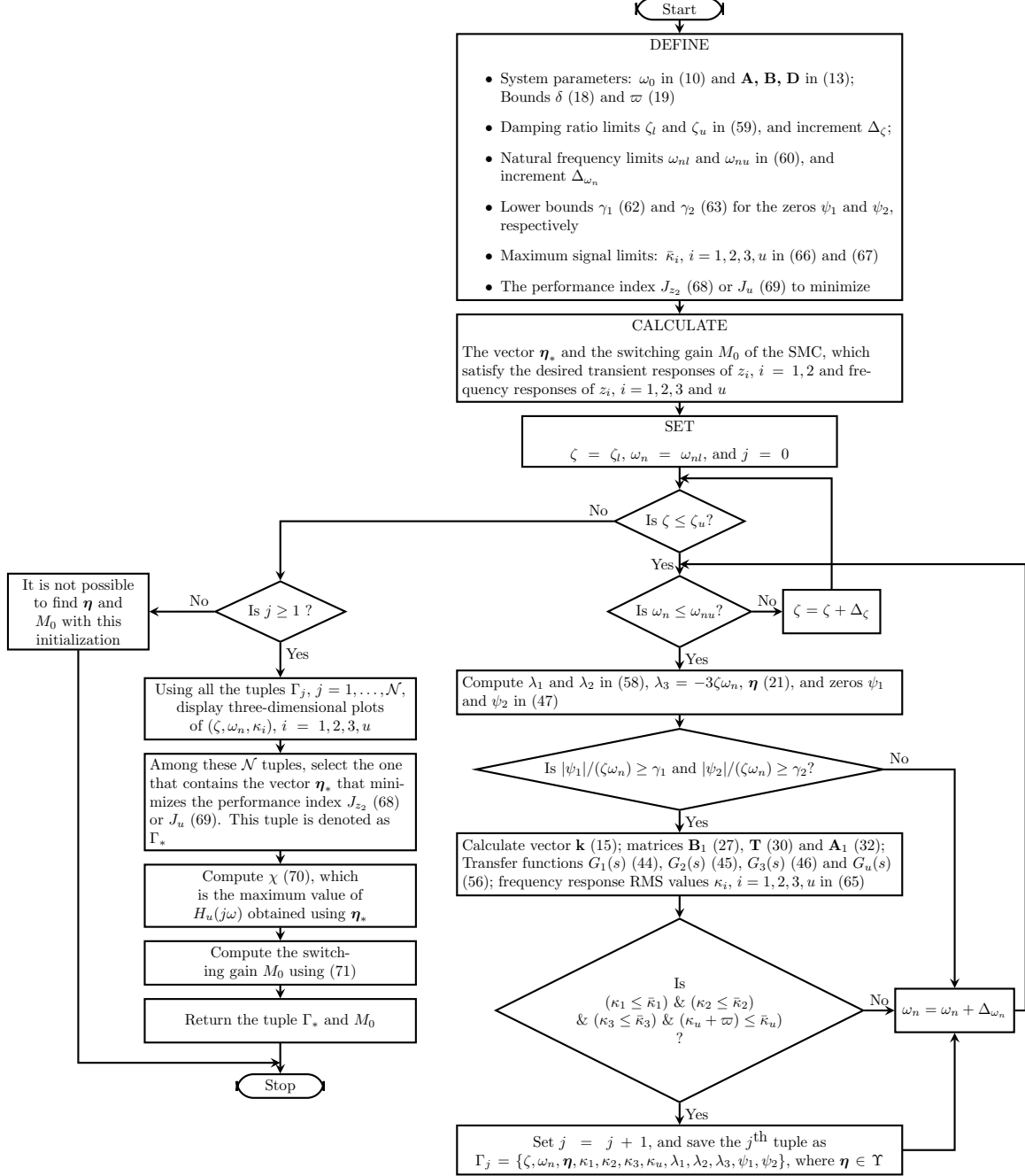


Figure 3: Proposed automatic tuning algorithm.

6. Results and discussion

The performance of the proposed tuning algorithm for the SMC, based on the Ackermann's formula, is evaluated by means of numerical and experimental studies. In both studies the SMC is programed in the Matlab/Simuink software and the data is sampled at 1 ms. The SMC in (20) causes the chattering effect [37], that is a discontinuous force at $\sigma = 0$ that cannot be applied to the ATMD in practice. To overcome it, the sign function of the SMC is approximated by means of following continuous saturation function

$$u = -M_0 \text{sign}(\sigma) \approx -M_0 \text{sat}(\sigma) = \begin{cases} -M_0 & \text{if } \sigma > \epsilon \\ \frac{\sigma}{\epsilon} & \text{if } -\epsilon \leq \sigma \leq \epsilon \\ M_0 & \text{if } \sigma < -\epsilon \end{cases} \quad (72)$$

where ϵ is a positive constant that is fixed to $\epsilon = 0.05$.

6.1. Numerical simulation

A reduced scale five-story building with an ATMD mounted on its top floor is simulated. The structure is excited through the North-South component of the El Centro (California, 1940) earthquake, whose magnitude has been scaled. The mass and stiffness of each floor are equal to 10 kg and 1.21×10^4 N/m, respectively. The mass m_0 and stiffness k_0 of the dominant first mode are 28.07 kg and 2.75×10^3 N/m, respectively. Therefore, the natural frequency of this mode is $\omega_0 = 9.9$ rad/s or $f_0 = 1.58$ Hz. It is assumed that the structure has Rayleigh damping, where the damping ratios of the first and second modes are equal to 0.01. The mass m_d of the ATMD is 1.4 kg, that is 5% of the modal mass m_0 . Moreover, the tuned parameters c_d and k_d are selected as $c_d = 3.54$ Ns/m and $k_d = 121.66$ N/m, which are the optimum parameters according to [38]. Using these parameters, the natural frequency $\omega_d = \sqrt{k_d/m_d}$ and damping ratio $\zeta_d = c_d/(2m_d\omega_d)$ of the ATMD are equal to $0.94\omega_0$ and 0.135, respectively. Finally, the function $f(z_3)$ in (13) is modeled as Coulomb friction acting between the ATMD and the floor on which it is attached. It is given by:

$$f(z_3) = \mu_d \text{sign}(z_3) \quad (73)$$

where μ_d is the Coulomb friction coefficient with a value of 0.35 N.

In order to compute the parameters η_* and M_0 of the SMC, the proposed tuning algorithm is initialized as follows: $\delta = 0.5$ m/s², $\varpi = 0.5$ N, $\gamma_1 = 5$ s, $\gamma_2 = 1$ s, $\zeta_l = 0.5$, $\zeta_u = 0.9$, $\Delta_\zeta = 0.01$, $\omega_{nl} = 0.5\omega_0$, $\omega_{nu} = \omega_0$, and $\Delta_{\omega_n} = 0.01$. Moreover, the signals z_1 , z_2 , z_3 and u are constrained using the bounds $\bar{\kappa}_1 = 20$ cm, $\bar{\kappa}_2 = 10$ mm, $\bar{\kappa}_3 = 70$ cm/s, and $\bar{\kappa}_u = 12$ N, respectively. The proposed algorithm displays three-dimensional surfaces of κ_1 , κ_2 , κ_3 and κ_u computed with the vectors $\eta \in \Upsilon$. These plots are shown in Figure 4 and they indicate that the feasible sets of parameters ζ and ω_n , that satisfy the desired transient responses of z_i , $i = 1, 2$ and frequency responses of z_i , $i = 1, 2, 3$ and u , are the intervals $[0.5 - 0.58]$ and $[0.5\omega_0 - 0.78\omega_0]$, respectively. The red point over the surfaces of κ_2 and κ_u indicates their minimum value. Table 1 presents the tuples $\Gamma_* = \{\zeta, \omega_n, \eta_*, \kappa_1, \kappa_2, \kappa_3, \kappa_u, \lambda_1, \lambda_2, \lambda_3, \psi_1, \psi_2\}$ and the switching gains M_0 returned by proposed algorithm by minimizing the performance indexes J_{z_2} and J_u .

Table 1: Tuples Γ_* returned by the proposed algorithm for the numerical structure.

PI	ζ	ω_n (rad/s)	η_*	κ_1 (cm)	κ_2 (mm)	κ_3 (cm/s)	κ_u (N)	λ_1 (rad/s)	λ_2 (rad/s)	λ_3 (rad/s)	ψ_1 (rad/s)	ψ_2 (rad/s)	M_0 (N)
J_{z_2}	0.5	$0.5\omega_0$	[2.6,-289.2, 0.87,-9.76]	4.0	1.0	33.8	5.76	-2.48 +4.29j	-2.48 -4.29j	-7.43	-29.64	-2.99	24.13
J_u	0.5	$0.62\omega_0$	[5,-312.3, 1.34,0.15]	3.7	1.4	31.4	3.68	-3.08 +5.33j	-3.08 -5.33j	-9.23	2114.6	-3.72	20.35

According to Figure 4 (b), the value of κ_2 monotonically increases with the increment of either ζ or ω_n , i.e., the minimum of κ_2 is located at (ζ_l, ω_{nl}) . Moreover, the mesh plot shown in Figure 4 (d) indicates that

the minimum of κ_u is located at $\zeta = \zeta_l$. Thus, using other initial parameters of ζ_l and ω_{nl} in the tuning algorithm changes the coordinates (ζ, ω_n) of the minimums of κ_2 and κ_u .

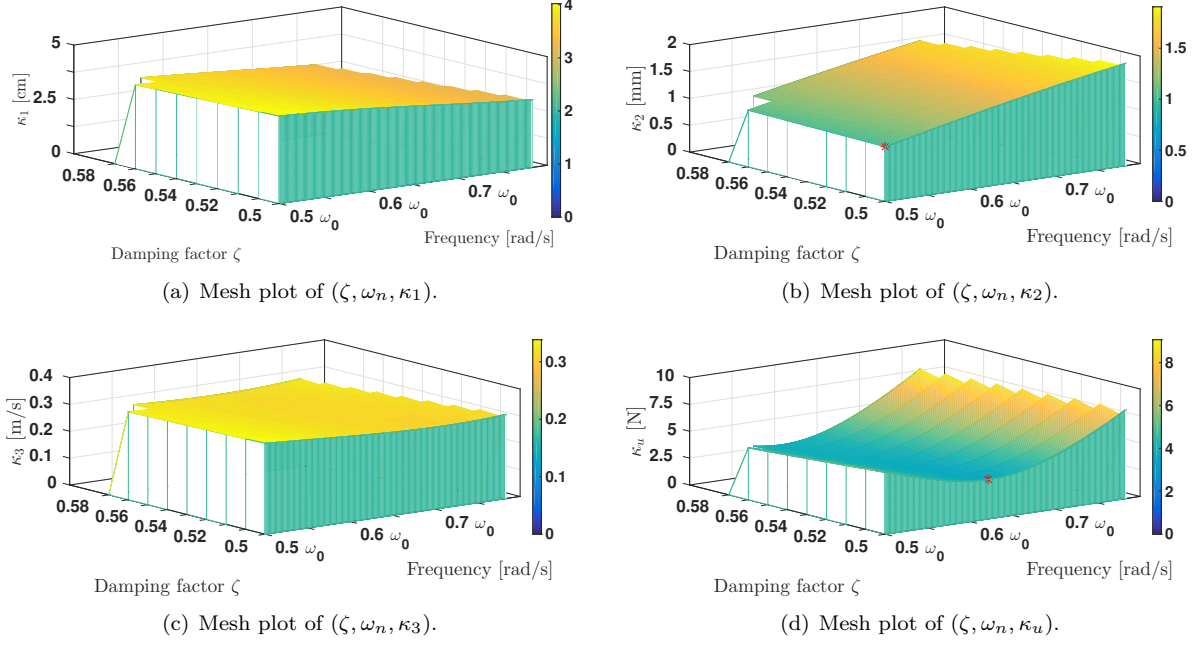


Figure 4: Three-dimensional surfaces of κ_1 , κ_2 , κ_3 and κ_u .

Figures 5 (a) and 5 (b) depict, respectively, the earthquake excitation signal \ddot{x}_g and the top floor displacement $x_5(t) = z_2(t)$ obtained using the TMD, i.e., with $u = 0$. Furthermore, Figures 6 (a), 6 (b), 7 (a), and 7 (b) presents, respectively, the signals z_1 , z_2 , z_3 and u , which are produced with the SMC using the parameters η_* and M_0 that minimize the PIs J_{z_2} and J_u . By comparing Figures 5 (b) and 6 (b), we can conclude that the ATMD, based on the proposed SMC and either of the PIs J_{z_2} and J_u , provides greater reduction of the building displacements when compared to the TMD.

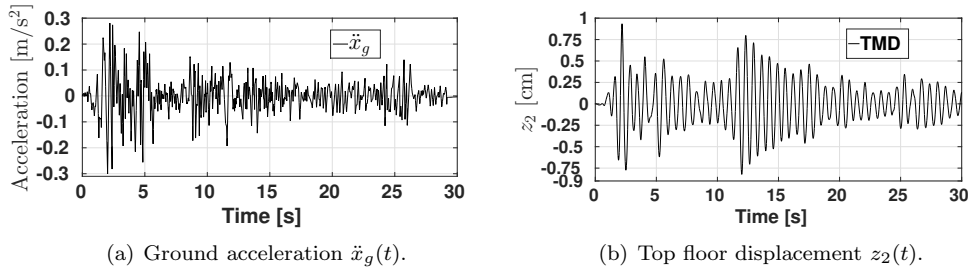


Figure 5: Signals $\ddot{x}_g(t)$ and z_2 .

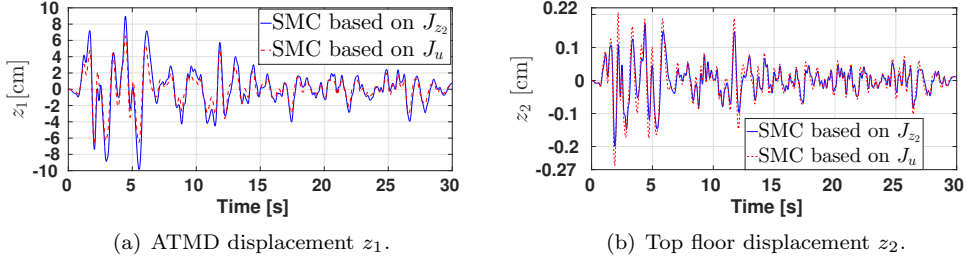


Figure 6: Displacements $z_1(t)$ and $z_2(t)$.

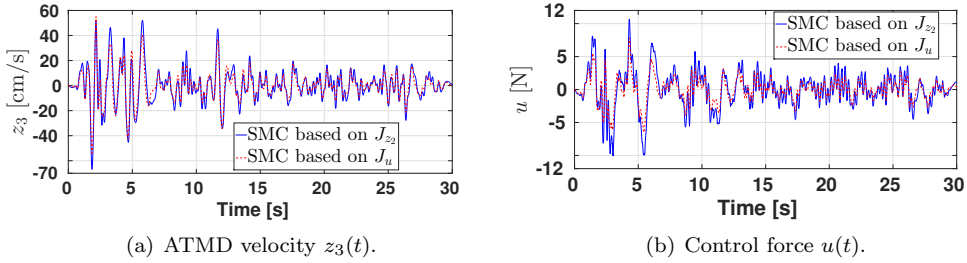


Figure 7: Signals $z_3(t)$ and $u(t)$.

Now, let us define z_i^{rms} , u^{rms} and z_i^{peak} , u^{peak} as the RMS and maximum peak values of signals z_i and u , respectively. Table 2 presents these values corresponding to the TMD and ATMD during the period of $t = 0$ to $t = 30$ s. This table indicates that the ATMD allows reducing more than three times the peak value of the floor displacement $z_2 = x_5$ when compared to the TMD. Note that the SMC that minimize the PI J_{z_2} (respectively J_u) produce the smallest z_2^{rms} (respectively u^{rms}), as expected. Finally, by comparing Tables 1 and 2, it is possible to observe that the values z_i^{rms} , $i = 1, 2, 3, u$ can be considered as an scaled version of the parameters κ_i , since the relation κ_i/z_i^{rms} is between 1.5 to 2.65.

Table 2: RMS and maximum peak values of z_i , $i = 1, 2, 3, 4$ and $u(t)$.

Damper	PI	z_1^{rms}	z_1^{peak}	z_2^{rms}	z_2^{peak}	z_3^{rms}	z_3^{peak}	z_4^{rms}	z_4^{peak}	u^{rms}	u^{peak}
		(cm)		(mm)		(cm/s)		(mm/s)		(N)	
TMD	—	0.33	1.33	2.67	9.33	3.19	13.38	25.8	93.8	0	0
ATMD	J_{z_2}	2.61	9.84	0.48	2.0	14.0	66.9	3.93	17.61	2.78	10.66
ATMD	J_u	1.86	6.74	0.58	2.58	11.81	55.04	5.11	26.49	1.81	7.81

6.2. Experimental results

Figure 8 shows the experimental structure, which was developed by the Quanser company. It consists of a single-story building controlled by an AMD, where the structure is mounted over a shake table, model STI-40. The maximum travel or stroke of the AMD is ± 9.5 cm. Moreover, the structure has an accelerometer that measures the floor acceleration, and two optical encoders to detect the AMD and the shake table displacements. The displacement z_2 and velocity z_4 of the story, as well as the velocity z_3 of the AMD are

estimated by means of a Luenberger state observer [39], that uses the measurements from the encoders and accelerometer. The SMC is programmed using the QUARC real-time control software of Matlab/Simulink. During the experiments, the structure is excited with the 1994 Northridge earthquake, which is scaled in time and amplitude, as shown in Figure 9. The model of the structure is given in (13), where $f(z_3)$ is given in (73). The parameters of the experimental structure are listed in Table 3, where c_d represents the viscous friction between the damper and the floor.

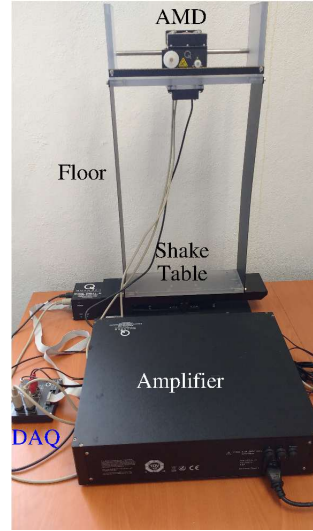


Figure 8: Experimental structure with an AMD.

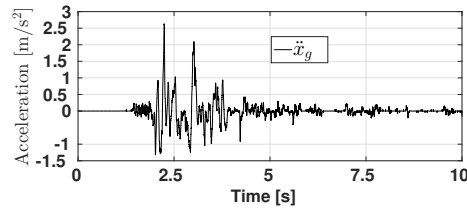


Figure 9: Shake table acceleration $\ddot{x}_g(t)$.

Table 3: Parameters of the experimental structure.

Parameter	Value	Units
m_0	1.84	kg
m_d	0.79	kg
k_0	226.23	N/m
k_d	0	N/m
c_0	0.16	N·s/m
c_d	6.85	N·s/m
μ_d	0.43	N
β_0	1	—
ω_0	11.08	rad/s

In order to compute the parameters M_0 and $\boldsymbol{\eta}_*$ of the SMC, the tuning algorithm is initialized with the parameters employed in the numerical simulation described in section 6.1, with the exception of parameter δ , that is set as $\delta = 3 \text{ m/s}^2$, and the maximum allowed values of signals z_1 , z_2 , z_3 and u , which are specified by means of the upper bounds $\bar{\kappa}_1 = 5 \text{ cm}$, $\bar{\kappa}_2 = 10 \text{ mm}$, $\bar{\kappa}_3 = 32 \text{ cm/s}$, and $\bar{\kappa}_u = 10 \text{ N}$, respectively. The tuning algorithm returns the mesh plots of κ_1 , κ_2 , κ_3 and κ_u , which are displayed in Figure 10 and indicate that the feasible intervals for ζ and ω_n are $[0.5 - 0.57]$ and $[0.5\omega_0 - 0.581\omega_0]$, respectively. The parameters returned by the proposed tuning algorithm are presented in Table 4.

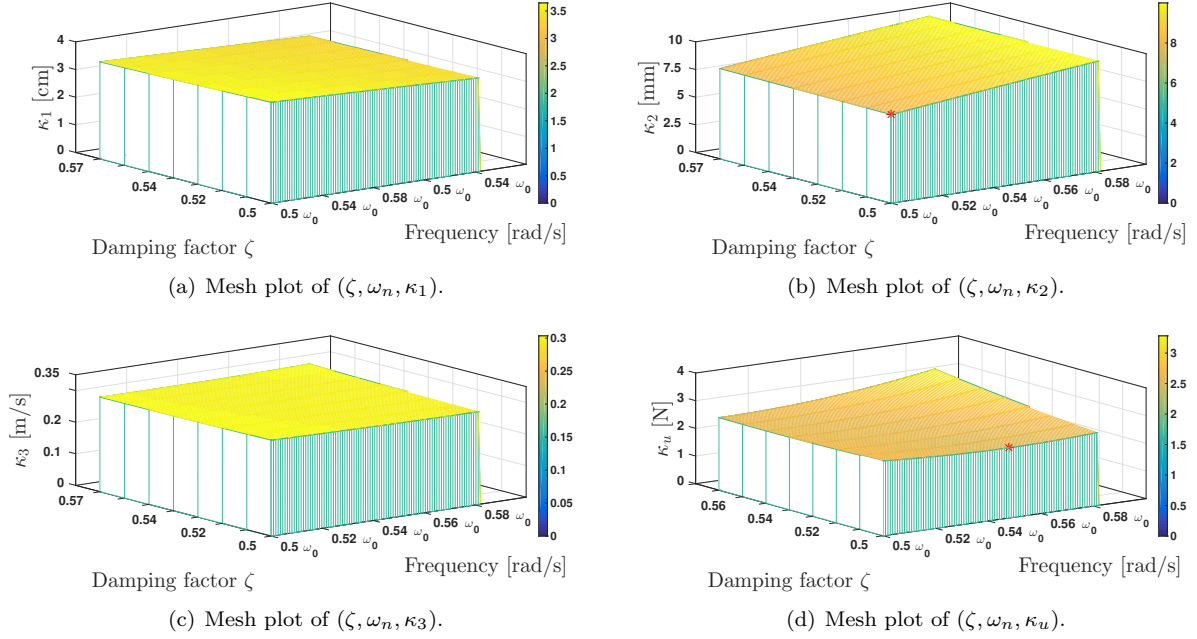


Figure 10: Three-dimensional surfaces of κ_1 , κ_2 , κ_3 and κ_u .

Table 4: Tuples Γ_* returned by the proposed algorithm for the experimental structure.

PI	ζ	ω_n (rad/s)	$\boldsymbol{\eta}_*$	κ_1 (cm)	κ_2 (mm)	κ_3 (cm/s)	κ_u (N)	λ_1 (rad/s)	λ_2 (rad/s)	λ_3 (rad/s)	ψ_1 (rad/s)	ψ_2 (rad/s)	M_0 (N)
J_{z_2}	0.5	$0.50\omega_0$	$[1.64, -19.94, 0.49, -0.20]$	3.65	8.0	30.33	2.71	-2.77 +4.8j	-2.77 -4.8j	-8.31	-99.15	-3.33	13.52
J_u	0.5	$0.55\omega_0$	$[2.16, -20.64, 0.59, 0.13]$	3.5	9.2	29.61	2.54	-3.04 +5.26j	-3.04 -5.26j	-9.11	162.45	-3.65	12.05

Figure 11 presents the frequency responses of the filters $H_i(j\omega, \boldsymbol{\eta}_*)$, $i = 1, 2, 3, u$ corresponding to the vectors $\boldsymbol{\eta}_*$ that minimize the PIs J_{z_2} and J_u . This figure also indicates the natural frequency of the structure $f_0 = \omega_0/(2\pi)$ in Hz. It shows that at low frequencies, the magnitude of $H_i(j\omega, \boldsymbol{\eta}_*)$ is larger than $\bar{\kappa}_i$; however, the RMS value κ_i of $H_i(j\omega, \boldsymbol{\eta}_*)$ is smaller than $\bar{\kappa}_i$ in the bandwidth of the earthquake \ddot{x}_g .

The proposed SMC is compared with the LQR [35], which minimizes the performance index

$$J_{\text{LQR}} = \int_0^\infty (\mathbf{z}^T \mathbf{Q} \mathbf{z} + r u^2) dt \quad (74)$$

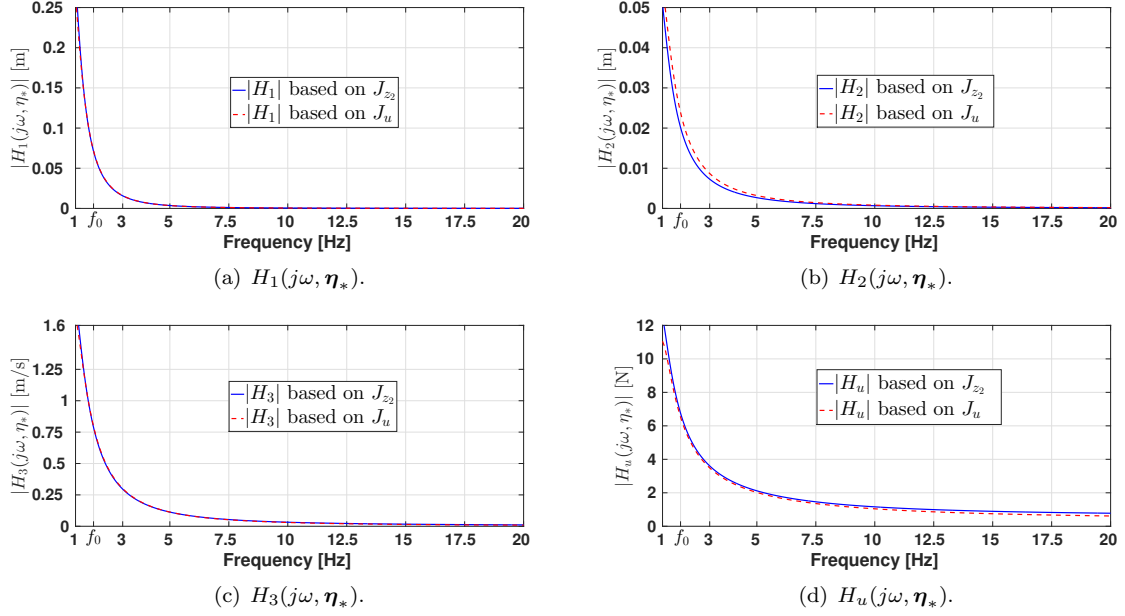


Figure 11: Frequencies responses $H_i(j\omega, \eta_*)$, $i = 1, 2, 3, u$ using the vector η_* that minimizes the PI J_{z_2} .

where $\mathbf{Q} \in \mathbb{R}^{4 \times 4}$ is a symmetric matrix such that $\mathbf{Q} \geq 0$; moreover r is a positive constant. Both \mathbf{Q} and r are designed according to the literature [35, 40], where the entries of $\mathbf{Q} = \text{diag}[q_{11}, q_{22}, q_{33}, q_{44}]$ satisfy

$$q_{ii} = \frac{1}{\text{maximum acceptable value of } z_i^2}, \quad i = 1, 2, 3, 4 \quad (75)$$

and the parameter r is given by

$$r = \frac{1}{\text{maximum acceptable value of } u^2} \quad (76)$$

The maximum acceptable values for z_i , $i = 1, 2, 3$ and u are, respectively, specified by the constants $\bar{\kappa}_j$, $j = 1, 2, 3, u$, which were mentioned above. The remaining maximum acceptable value for z_4 is chosen as 0.1 m/s. Thus, coefficients q_{ii} , $i = 1, 2, 3, 4$ in (75) and r in (76) are given by:

$$q_{11} = 400, \quad q_{22} = 10,000, \quad q_{33} = 9.77, \quad q_{44} = 100, \quad r = 0.01 \quad (77)$$

The control law u that minimizes the performance index J_{LQR} in (74) is computed as

$$u = -\mathbf{k}_J \mathbf{z} \quad (78)$$

where $\mathbf{k}_J = \frac{1}{r} \mathbf{B}^T \mathbf{P}$ and $\mathbf{P} = \mathbf{P}^T > 0$ is the solution of the Riccati equation

$$\mathbf{A}^T \mathbf{P} + \mathbf{P} \mathbf{A} - \frac{1}{r} \mathbf{P} \mathbf{B} \mathbf{B}^T \mathbf{P} = -\mathbf{Q} \quad (79)$$

Solving (79) yields $\mathbf{k}_J = [200, -1276.5, 49, 17.32]$, and the closed-loop eigenvalues $\lambda_1 = -3.52 + j6.82$, $\lambda_2 = -3.52 - j6.82$, $\lambda_3 = -6.77$ and $\lambda_4 = -77.98$. Using these dominant poles λ_1 and λ_2 permits computing the parameters ζ and ω_n of the closed-loop system, which are $\zeta = 0.46$ and $0.69\omega_0$. Note that these LQR parameters do not belong to the feasible intervals of ζ and ω_n corresponding to the SMC.

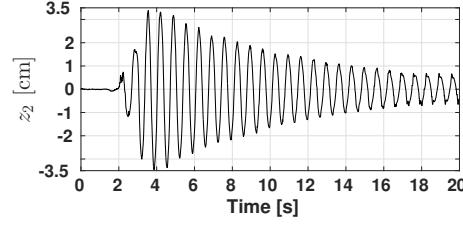


Figure 12: Uncontrolled response of $z_2(t)$.

Figure 12 depicts the uncontrolled response $z_2(t)$ of the structure under the earthquake excitation, which indicates that its maximum magnitude is approximately 3.5 cm. On the other hand, Figures 13 (a), 13 (b), 14 (a), 14 (b) and 15 show, respectively, the signals $z_1(t)$, $z_2(t)$, $z_3(t)$, $z_4(t)$ and $u(t)$ produced by the LQR and the SMC. From these plots, it is possible to see that the maximum displacement $z_2(t)$ corresponding to the SMC, based on either PI J_{z_2} or J_u , is smaller than that produced by the LQR controller. Moreover, the maximum peak of signals $u(t)$ and $z_1(t)$ corresponding to the SMC is slightly larger than the one generated by the LQR controller, but these signals are within the specified limits.

In addition, Table 5 presents the RMS and maximum peak values of the signals $u(t)$ and z_i , $i = 1, 2, 3, 4$ corresponding to the SMC and LQR, during the period of $t = 2$ to $t = 6$ s. Note that the relations κ_i/z_i^{rms} , $i = 1, 2, 3, u$, are between 2.15 to 4.54. This table indicates that the SMC and LQR allow attenuating more than three times the peak of the uncontrolled response of z_2 . Moreover, the SMC that minimizes the PI J_{z_2} produces the smaller RMS value of z_2 , as expected. Note also, that the value z_2^{rms} corresponding to the SMC based on the PI J_u is smaller than that produced by the LQR, and their corresponding control efforts u^{rms} are similar. These results show that the SMC based on the Ackermann's formula and either of the PIs J_{z_2} or J_u has great potential for active structural control.

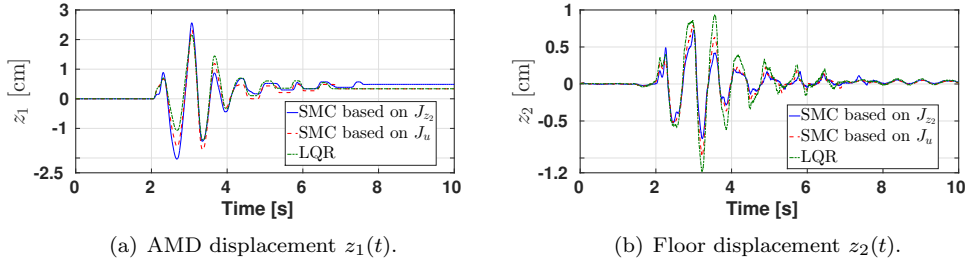


Figure 13: Displacements of the AMD and floor.

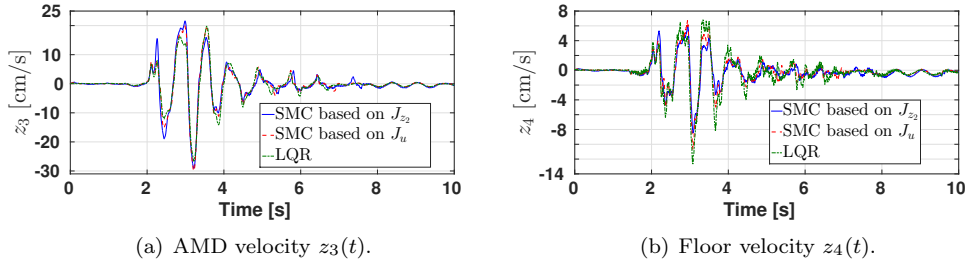


Figure 14: Velocities of the AMD and floor.

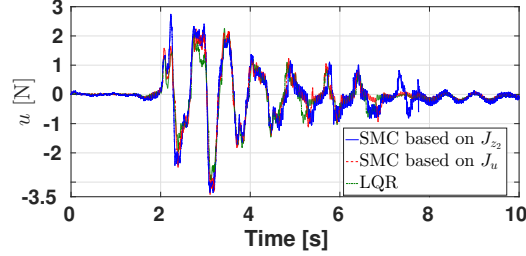


Figure 15: Control force generated by SMC and LQR.

Table 5: RMS and maximum peak values of z_i , $i = 1, 2, 3, 4$ and $u(t)$.

Controller	PI	z_1^{rms}	z_1^{peak}	z_2^{rms}	z_2^{peak}	z_3^{rms}	z_3^{peak}	z_4^{rms}	z_4^{peak}	u^{rms}	u^{peak}
		(cm)		(mm)		(cm/s)		(cm/s)		(N)	
Control OFF	—	—	—	20.14	35.31	—	—	17.90	34.54	—	—
SMC	J_{z_2}	0.84	2.56	2.62	7.39	9.59	29.06	2.52	8.49	1.25	3.36
SMC	J_u	0.77	2.32	3.21	9.73	9.39	29.95	2.89	10.71	1.18	3.43
LQR	J_{LQR}	0.74	2.17	4.21	11.80	8.75	26.62	3.50	12.68	1.05	2.92

7. Conclusions

This paper proposed a tuning algorithm for a SMC designed for attenuating the structural vibration of a seismically excited building equipped with an ATMD on its top floor. The SMC is derived based on the Ackermann's formula and its robustness against friction uncertainty was demonstrated. It was proved that the seismic excitation signal is not a coupled disturbance, and as consequence it cannot be eliminated by the SMC; however, its effect can be minimized by designing the SMC with the proposed tuning algorithm.

It was also shown that the responses of the ATMD and building under the SMC can be described by means of dominant second-order filters, whose input is the seismic excitation. Their parameters were automatically tuned by the proposed algorithm in order to minimize the PI J_{z_2} or J_u . The PI J_{z_2} is related to the minimization of the top floor displacement, while the PI J_u is related to the minimization of the control force applied the ATMD while offering a great attenuation of this displacement. The effectiveness of the designed SMC was demonstrated in a numerical and an experimental structure. Moreover, the experiments showed that the designed SMC has a better vibration attenuation performance than the LQR, while ensuring that the structure and the ATMD signals are within the specified limits.

References

- [1] S.-Y. Kim, C.-H. Lee, Peak response of frictional tuned mass dampers optimally designed to white noise base acceleration, *Mechanical Systems and Signal Processing* 117 (2019) 319–332.
- [2] S. Chesne, G. Inquieté, P. Cranga, F. Legrand, B. Petitjean, Innovative hybrid mass damper for dual-loop controller, *Mechanical Systems and Signal Processing* 115 (2019) 514–523.
- [3] S. Paul, W. Yu, A method for bidirectional active control of structures, *Journal of Vibration and Control* 24 (15) (2018) 3400–3417.
- [4] A. E. Kayabekir, G. Bekdaş, S. M. Nigdeli, Z. W. Geem, Optimum design of pid controlled active tuned mass damper via modified harmony search, *Applied Sciences* 10 (8) (2020) 2976.

- [5] D.-H. Yang, J.-H. Shin, H. Lee, S.-K. Kim, M. K. Kwak, Active vibration control of structure by active mass damper and multi-modal negative acceleration feedback control algorithm, *Journal of Sound and Vibration* 392 (2017) 18–30.
- [6] E. Talib, J.-H. Shin, M. K. Kwak, Designing multi-input multi-output modal-space negative acceleration feedback control for vibration suppression of structures using active mass dampers, *Journal of Sound and Vibration* 439 (2019) 77–98.
- [7] A. Younespour, H. Ghaffarzadeh, Structural active vibration control using active mass damper by block pulse functions, *Journal of Vibration and Control* 21 (14) (2015) 2787–2795.
- [8] C. Chang, H. T. Yang, Control of buildings using active tuned mass dampers, *Journal of engineering mechanics* 121 (3) (1995) 355–366.
- [9] S. Ankireddi, H. T. Y. Yang, Simple atmd control methodology for tall buildings subject to wind loads, *Journal of Structural Engineering* 122 (1) (1996) 83–91.
- [10] Y. Xu, H. Hua, J. Han, Modeling and controller design of a shaking table in an active structural control system, *Mechanical Systems and Signal Processing* 22 (8) (2008) 1917–1923.
- [11] C. Li, J. Li, Y. Qu, An optimum design methodology of active tuned mass damper for asymmetric structures, *Mechanical Systems and Signal Processing* 24 (3) (2010) 746–765.
- [12] F. Ricciardelli, A. D. Pizzimenti, M. Mattei, Passive and active mass damper control of the response of tall buildings to wind gustiness, *Engineering structures* 25 (9) (2003) 1199–1209.
- [13] Z.-H. Li, C.-J. Chen, J. Teng, A multi-time-delay compensation controller using a Takagi–Sugeno fuzzy neural network method for high-rise buildings with an active mass damper/driver system, *The Structural Design of Tall and Special Buildings* 28 (13) (2019) e1631.
- [14] Y. Lei, J. Lu, J. Huang, S. Chen, A general synthesis of identification and vibration control of building structures under unknown excitations, *Mechanical Systems and Signal Processing* 143 (2020) 106803.
- [15] S. Allaoua, L. Guenaf, LQG vibration control effectiveness of an electric active mass damper considering soil–structure interaction, *International Journal of Dynamics and Control* 7 (1) (2019) 185–200.
- [16] B.-L. Zhang, Y.-J. Liu, Q.-L. Han, G.-Y. Tang, Optimal tracking control with feedforward compensation for offshore steel jacket platforms with active mass damper mechanisms, *Journal of Vibration and Control* 22 (3) (2016) 695–709.
- [17] B. Spencer Jr, J. Suhardjo, M. Sain, Frequency domain optimal control strategies for aseismic protection, *Journal of Engineering Mechanics* 120 (1) (1994) 135–158.
- [18] R. B. Santos, D. D. Bueno, C. R. Marqui, V. Lopes Jr, Active vibration control of a two-floors building model based on H_2 and H_∞ methodologies using linear matrix inequalities (lmis)., in: *International Modal Analysis Conference–XXV IMAC*, Orlando, EUA, 2007, pp. 1–13.
- [19] L. Xu, Y. Yu, Y. Cui, Active vibration control for seismic excited building structures under actuator saturation, measurement stochastic noise and quantisation, *Engineering Structures* 156 (2018) 1–11.
- [20] S.-M. Yang, C.-J. Chen, W. Huang, Structural vibration suppression by a neural-network controller with a mass-damper actuator, *Journal of Vibration and Control* 12 (5) (2006) 495–508.
- [21] S. Thenozhi, W. Yu, Active vibration control of building structures using fuzzy proportional-derivative/proportional-integral-derivative control, *Journal of Vibration and Control* 21 (12) (2015) 2340–2359.
- [22] Q. Li, D. Liu, J. Fang, C. Tam, Multi-level optimal design of buildings with active control under winds using genetic algorithms, *Journal of Wind Engineering and Industrial Aerodynamics* 86 (1) (2000) 65–86.
- [23] A. Banaei, J. Alamatian, New genetic algorithm for structural active control by considering the effect of time delay, *Journal of Vibration and Control* (2020) 1077546320933467.
- [24] J. Yang, J. Wu, A. Agrawal, Sliding mode control for seismically excited linear structures, *Journal of engineering mechanics* 121 (12) (1995) 1386–1390.
- [25] R. Adhikari, H. Yamaguchi, Sliding mode control of buildings with ATMD, *Earthquake Engineering & Structural Dynamics* 26 (4) (1997) 409–422.
- [26] A.-P. Wang, Y.-H. Lin, Vibration control of a tall building subjected to earthquake excitation, *Journal of Sound and Vibration* 299 (4-5) (2007) 757–773.
- [27] L. Li, N. Wang, H. Qin, Adaptive model reference sliding mode control of structural nonlinear vibration, *Shock and Vibration* 2019.
- [28] M. Soleymani, A. H. Abolmasoumi, H. Bahrami, A. Khalatbari-S, E. Khoshbin, S. Sayahi, Modified sliding mode control of a seismic active mass damper system considering model uncertainties and input time delay, *Journal of Vibration and Control* 24 (6) (2018) 1051–1064.
- [29] N. Mamat, F. Yakub, S. A. Z. Shaikh Salim, M. S. Mat Ali, Seismic vibration suppression of a building with an adaptive nonsingular terminal sliding mode control, *Journal of Vibration and Control* (2020) 1077546320915324.
- [30] A. K. Chopra, *Dynamics of Structures: theory and applications to earthquake engineering*, Prentice Hall, Englewood Cliffs, NJ, 2001.
- [31] W. Yu, S. Thenozhi, *Active structural control with stable fuzzy PID techniques*, Springer, 2016.
- [32] J. Wu, J. Yang, W. Schmitendorf, Reduced-order H_∞ and LQR control for wind-excited tall buildings, *Engineering Structures* 20 (3) (1998) 222–236.
- [33] J. Ackermann, *Sampled-Data Control Systems*, Springer-Verlag, Berlin, Germany, 1985.
- [34] J. Ackermann, V. Utkin, Sliding mode control design based on Ackermann’s formula, *IEEE Transactions on Automatic Control* 43 (2) (1998) 234–237.
- [35] G. F. Franklin, J. D. Powell, A. Emami-Naeini, J. D. Powell, *Feedback control of dynamic systems*, 7th Edition, Pearson, Upper Saddle River, NJ, 2015.
- [36] J. Kayal, *Microearthquake seismology and seismotectonics of South Asia*, Springer Science & Business Media, 2008.
- [37] J. E. Slotine, W. Li, *Applied Nonlinear Control*, Prentice Hall, 2002.

- [38] R. Rana, T. Soong, Parametric study and simplified design of tuned mass dampers, *Engineering structures* 20 (3) (1998) 193–204.
- [39] K. Ogata, *Modern control engineering*, Prentice Hall, Upper Saddle River, NJ, 2002.
- [40] A. E. Bryson, Y. C. Ho, *Applied Optimal Control*, Taylor & Francis, Madison Avenue, NY, 1975.